

INFLUENCE OF SYNTHESIS pH ON KAOLINITE “CRYSTALLINITY” AND SURFACE PROPERTIES

CLAIRE-ISABELLE FIALIPS, SABINE PETIT, ALAIN DECARREAU, AND DANIEL BEAUFORT

Laboratoire Hydr’ASA, UMR6532-CNRS, Université de Poitiers, 40 avenue du Recteur Pineau, F-86022 Poitiers Cedex, France

Abstract—Hydrothermal syntheses were performed at various pH values and temperatures to induce variability in kaolinite defect density. Temperature of synthesis ranged from 200 to 240°C, for 21 d. Initial pH at room temperature ranged from 0.5 to 14. The starting material was a hydrothermally treated gel, with an atomic Si/Al ratio of 0.93, partly transformed into kaolinite.

Kaolinite was obtained for a wide range of pH. Although no influence of temperature on “crystallinity” (*i.e.*, defect density) was observed, the effect of pH was important. A continuous series was obtained from a low-defect kaolinite, with high thermal stability and a hexagonal morphology for the most acidic final pH, to a high-defect kaolinite, with low thermal stability and lath shape for the most basic final pH. These variations of kaolinite properties appear related to the pH dependence of kaolinite surface speciation. Increasing pH value results in increased cation adsorption on the kaolinite external surfaces and increases in the elongation of particles.

Key Words—Defect Density, FTIR, Hydrothermal Synthesis, Kaolinite, pH, Surface Speciation, XRD.

INTRODUCTION

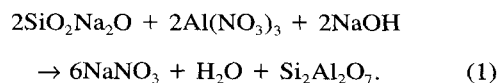
Although the kaolin subgroup has been studied extensively during the last 70 years, crystallization conditions remain only partly known. Despite many experiments to synthesize kaolinite at room temperature from solutions or noncrystalline materials (Van Oosterwyck-Gastuche and La Iglesia, 1978), only Espiau and Pedro (1984) obtained unquestionably a kaolin mineral after a relatively short time (three months). Thus, kaolinite syntheses were mainly performed under hydrothermal conditions ($\geq 200^\circ\text{C}$). Rayner (1962) studied the kinetic effect of temperature and synthesis duration on the rate of kaolinite formation from a (non-crystalline) gel. Huertas *et al.* (1993) established that the increase of temperature and duration of kaolinite hydrothermal synthesis improves “crystallinity” (*i.e.*, reduces the defect density). However, after a certain synthesis time (~ 15 d at 225°C), no increase in the amount of kaolinite or decrease in defect density is observed. Tomura *et al.* (1985) and Fiore *et al.* (1995) established that as temperature and/or duration of synthesis increased, the amount of lath-shaped or platy kaolinite increased. They also observed the formation of rose-shaped aggregates and a decrease in the number of kaolinite spherules with increasing temperature. The role of pH in kaolinite synthesis from various starting products was investigated by De Kimpe *et al.* (1964), La Iglesia Fernandez and Martin Vivaldi (1973), Eberl and Hower (1975), and Satokawa *et al.* (1994, 1996). Acidic conditions, depending upon the starting material, favor kaolinite crystallization and can improve “crystallinity”. However, kaolinite defect density (Satokawa *et al.*, 1996) was assessed only within a small range of final pH (0.4–4.8).

Most studies used an amorphous gel or minerals such as feldspars; none used a gel already partially crystallized to kaolinite. Such an approach may allow the observation of kaolinite crystal growth. In the present study, kaolinite was hydrothermally synthesized from starting material partially crystallized into kaolinite. Hydrothermal syntheses of kaolinite were performed for 21 d, from 200 to 240°C , and pH from 0.5 to 14. The defect density and the morphology of the synthesized kaolinites were studied with respect to pH and temperature.

MATERIALS

Starting material

An initial gel was prepared with 0.2 M sodium metasilicate ($\text{SiO}_2\text{Na}_2\text{O}\cdot 5\text{H}_2\text{O}$), 0.2 M aluminum nitrate [$\text{Al}(\text{NO}_3)_3\cdot 9\text{H}_2\text{O}$] and 1 M sodium hydroxide added according to the following reaction:



After completion, the coprecipitate was centrifuged to remove sodium nitrate. The gel was then dehydrated at 70°C for 12 h and crushed. It was X-ray amorphous. The silicoaluminous gel was hydrothermally treated with distilled water at 220°C ($\pm 3^\circ\text{C}$), under equilibrium water pressure (23.2 bar), for 14 d. The initial pH was ~ 5 . This partially crystallized gel was then used as starting material for kaolinite synthesis.

The expected atomic ratio Si/Al/Na of the starting material is 2/2/0 (kaolinite stoichiometry). The measured atomic ratio Si/Al/Na is 2.00/2.15/0.07, showing a small excess in aluminum owing to the fact that Reaction (1) did not go to completion.

Table 1. Synthesis conditions and crystalline data of the starting material and of synthesized kaolinites.

T (±3°C)	pH _i (±0.2)	pH _f (±0.2)	Parageneses	CS ₀₀₁ (±20 Å)	CS ₀₆₀ (±15 Å)	HI	R ₂	T _{max} (±5°C)
—	—	—	¹ Kaol + Am + (PBoehm)	263	238	0.85(8)	0.4 (1)	501
200	2.0	2.0	Kaol + PBoehm	286	240	0.99(6)	0.53(4)	518
200	4.5	5.5	Kaol	271	241	0.86(5)	0.40(4)	511
200	5.5	5.7	Kaol	285	241	0.86(6)	0.45(6)	512
200	6.0	5.6	Kaol	254	236	0.87(4)	0.42(5)	510
200	6.5	5.8	Kaol	252	244	0.85(5)	0.45(5)	511
200	8.1	5.7	Kaol	262	243	0.97(5)	0.44(4)	511
200	10.4	6.1	Kaol + (PBoehm)	250	249	0.86(4)	0.52(5)	510
200	11.5	7.3	Kaol + (PBoehm) + (Am)	181	226	0.5 (1)	0.33(9)	496
200	12.6	12.4	Hydr Neph I + (Cancr)	—	—	—	—	—
220	0.5	0.5	Si	—	—	—	—	—
220	1.0	1.1	Kaol + ((PBoehm))	286	242	0.99(5)	0.65(5)	516
220	2.0	2.2	Kaol + (PBoehm)	276	240	0.87(5)	0.52(5)	515
220	4.5	5.5	Kaol	262	243	0.90(4)	0.42(5)	511
220	5.5	5.9	Kaol	259	242	0.85(5)	0.42(5)	508
220	6.0	5.9	Kaol	253	249	0.85(5)	0.41(5)	514
220	6.5	6.0	Kaol	260	236	0.91(5)	0.43(5)	512
220	11.5	8.4	Kaol + (PBoehm) + (Am)	227	224	0.6 (2)	0.4 (1)	502
220	14.0	13.7	Hydr Neph I + Cancr	—	—	—	—	—
240	0.5	0.6	Si	—	—	—	—	—
240	1.0	1.0	Kaol	293	251	1.09(5)	0.81(5)	525
240	2.1	2.1	Kaol + PBoehm	276	251	1.02(6)	0.62(5)	517
240	3.6	4.0	Kaol + ((PBoehm))	295	244	0.97(8)	0.61(7)	518
240	5.1	4.7	Kaol + ((PBoehm))	276	251	0.96(6)	0.50(6)	516
240	6.4	5.7	Kaol	288	251	0.99(7)	0.54(7)	512
240	8.1	5.6	Kaol	268	262	1.02(5)	0.50(5)	514
240	10.7	6.6	Kaol + ((PBoehm)) + ((Am))	239	261	0.99(9)	0.5 (1)	508
240	12.8	7.9	Kaol + PBoehm + (Parag) + ((Am))	237	199	0.8 (3)	0.5 (3)	496

¹ Starting material.

T = temperature of synthesis; pH_i, pH_f = initial and final pH; CS₀₀₁, CS₀₆₀, HI, R₂, T_{max} = see text; Kaol = kaolinite; PBoehm = pseudoboehmite; Si = amorphous silica; Am = amorphous product; Parag = paragonite; Hydr Neph I = hydrated nepheline of I type (Na₂Al₂Si₂O₈·xH₂O, Barrer and White, 1952); Cancr = cancrinite [Na₄₋₈(Al, Si)₁₂O₂₄(CO₃)₁₋₂]. () = minor phase; (()) = trace.

Analyses of the starting material showed that it contained kaolinite of medium “crystallinity” based on the Hinckley index (Hinckley, 1963) (Table 1). The starting material also contained amorphous product and a small amount of pseudoboehmite. The amount of pseudoboehmite was not determined because this phase is poorly crystallized and the temperature of dehydroxylation is close to that of kaolinite (Tettenhorst and Hofmann, 1980). Thermogravimetric analysis suggested ~50% kaolinite in the product.

Hydrothermal aging

An amount of 400 mg of powdered starting material and 30 mL of distilled water were placed in experimental vessels with metal bodies and removable Teflon liners. In some cases, hydrochloric acid or sodium hydroxide was added to produce an initial pH (pH_i) within the range 0.5–14. This pH_i was adjusted and measured directly in the vessel, after mixing and stabilization, at room temperature. Vessels were held at 200, 220, or 240°C (±3°C), under equilibrium water pressure (respectively, 15.5, 23.2, and 33.5 bar). Synthesis duration was 21 d. Final pH (pH_f) values were measured on quenched synthesis fluids.

METHODS

Chemical analyses of synthetic samples were performed by atomic absorption spectrometry (AAS) with a Perkin Elmer 2380 spectrometer, for silicon, aluminum, and sodium. Samples were prepared by fusion with strontium metaborate and dissolution in nitric acid (Jeanroy, 1974).

Ammonium saturation of the samples was performed in 1 mL of 1 M ammonium acetate solution, agitated, and aged for 2 h. Samples were then removed from the solution by centrifugation, again suspended in 1 mL of the ammonium acetate solution, and aged 2 h. The NH₄-saturated samples were washed until free of ammonium salts (*i.e.*, until no reaction with the reagent of Nessler HgI₄K₂).

X-ray diffraction (XRD) patterns were obtained with a Philips PW 1050/25 DY 5249 diffractometer equipped with Ni-filtered CuK α radiation (40 kV, 40 mA), combined with a SOCBIM system (DACOMP) for numerical data acquisition. Measurements were performed on randomly oriented powder preparations except for the characterization of pseudoboehmite which, in some cases, required oriented prepa-

rations. Defects in kaolinite (Hinckley, 1963) were characterized using the Hinckley index (HI) and the R_2 index of Liétard (Liétard, 1977; Cases *et al.*, 1982). The R_2 value was calculated from the intensities of the (131) and ($\bar{1}31$) reflections, in the range 37–40 °2 θ CuK α . The apparent coherent scattering thickness of kaolinite was calculated along the c^* axis, using the (001) reflection (CS_{001}) and along the b axis using the (060) reflection (CS_{060}), according to the Scherrer formula (Guinier, 1956).

An electrobalance NETZSCH STA 409 EP was used for thermodifferential and thermogravimetric (DTA-TG) analyses. The DTA-TG thermocouple was calibrated using seven standard minerals with well-known onset temperatures (*e.g.*, Li₂SO₄; onset temperature of 578.1°C). The measurements were performed with ~20 mg of sample, heated in air, at 10°C/min, from 20 to 1100°C. The temperature of kaolinite dehydroxylation (T_{max}) is measured at the maximum deviation from background of the endotherm. TG analyses allowed estimation of the percentage of kaolinite present in each product (% Kaol). % Kaol was calculated by comparing the water loss of the sample (in wt. %) within the temperature ranges of 25–350°C (molecular water) and 350–800°C (kaolinite dehydroxylation), with the theoretical water loss (14 wt. %) of an ideal kaolinite.

Morphological observations of the synthesized products were made by transmission electron microscopy (TEM) with a JEOL 100CX microscope, operating at 80 kV, using samples dispersed in distilled water and sedimented on carbon-coated Cu-microgrids.

Fourier-transform infrared (FTIR) spectra were recorded in the 400–4000-cm⁻¹ range on a Nicolet 510 FTIR spectrometer with a 4-cm⁻¹ resolution. They were obtained by transmission mode from KBr pressed pellets, which were previously heated at 110°C overnight. These pellets were prepared by homogeneous mixing of 3–4 mg of sample with 300 mg of KBr. Kaolinite FTIR spectra were normalized by equalizing the total integrated intensity of the Si–O–^{VI}Al band located at 538–542 cm⁻¹ (Stubican and Roy, 1961; Pampuch, 1966; Hlavay *et al.*, 1977) to an arbitrarily chosen value to allow a quantitative comparison of the samples. The measurements of the integrated intensity of the absorption bands were made with OMNIC software from Nicolet Instrument. FTIR spectra of NH₄⁺-saturated samples were obtained to evaluate the amount of adsorbed ammonium on kaolinite using the NH₄⁺-deformation band (ν_4 NH₄) located at 1400 cm⁻¹ (Nakamoto, 1963; Vedder, 1965), according to Petit *et al.* (1999).

RESULTS

Parageneses, “crystallinity” data, and synthesis conditions are given in Table 1. Kaolinite was obtained

within a wide range of pH for pH_i = 1–13 at 240°C, and 11.5 at 200 and 220°C, with corresponding pH_F of 1–8.4. Kaolinite was sometimes associated with minor amounts of pseudoboehmite. Remnant amorphous products were detected only for the most basic pH_F. For these samples, % Kaol was estimated at 60–70%. For all other samples, kaolinite crystallization was 90–100%. Feldspathoidic minerals were formed for pH_F > 12 and amorphous silica was the only phase obtained for pH_F < 1.

XRD

The powder XRD patterns of kaolinite synthesized at 220°C are shown in Figure 1 according to pH_F. For pH_F ≤ 5.5, reflections are narrow and intense, indicating low-defect density (Brindley and Brown, 1980). Small amounts of pseudoboehmite are detected for pH_F = 1.1 and 2.2. For pH_F = 8.4, kaolinite is observed but is poorly crystallized (note broad diffraction hump at 20–35 °2 θ); it is associated with a small amount of pseudoboehmite. This pseudoboehmite shows a broad peak at 6–7 °2 θ (Figure 2, curve a) which shifts to 4–5 °2 θ after ethylene glycol treatment (Figure 2, curve b), but disappears after heating at 120°C for 2 h (Figure 2, curve c). Tettenhorst and Hofmann (1980) described a similar synthetic expandable pseudoboehmite. The pseudoboehmite obtained at 240°C and pH_F = 7.9 (not shown) does not show the same swelling properties, and it is associated with a synthetic 1M polytypic form of paragonite (Chatterjee, 1970).

When the $\bar{1}31$ and 131 reflections of kaolinite are well resolved, then a marked triclinic character is indicated but when only one apparent peak occurs, then monoclinic character is indicated (Plançon and Tchoubar, 1977; Liétard, 1977; Brindley and Porter, 1978). XRD patterns (Figure 1) indicate that the monoclinic character of the synthesized kaolinites increases with increasing pH_F value at ≤5.5. This trend seems independent of temperature of synthesis (200, 220, or 240°C). For pH_F = 8.4, the loss of resolution does not necessarily mean that the symmetry has changed, but just that there is an increased mosaic character probably owing to particle-size changes.

“Crystallinity” indexes (HI and R_2) and apparent coherent scattering thickness (CS_{001} and CS_{060}) of the synthesized kaolinites are plotted vs. pH_F in Figures 3 and 4, respectively. The temperature, within 200–240°C, does not have any influence on either “crystallinity” indexes or apparent coherent scattering thickness of kaolinites.

The “crystallinity” indexes obtained are in the range of those of natural occurring kaolinites, which can approach 1.5 for HI and 1.2 for R_2 (Liétard, 1977). HI (Figure 3a) is almost constant or only slightly decreases as pH_F increases. Only three samples have a significantly lower HI (for the higher pH_F), but stan-

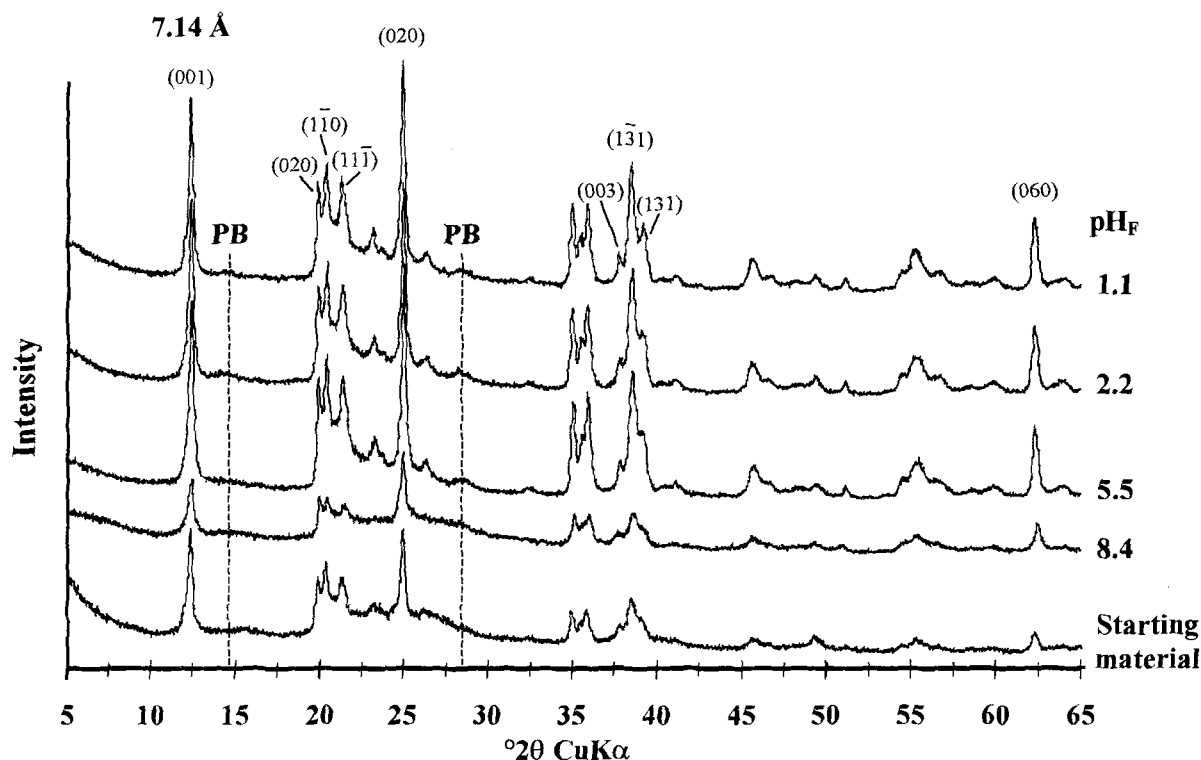


Figure 1. XRD patterns of the starting material and of the products synthesized at 220°C according to pH_F . PB = Pseudo-boehmite.

standard deviations are large owing to the presence of the broad diffraction hump between 20–35 $^{\circ}2\theta$. Moreover, for the sample synthesized at 240°C for $\text{pH}_F = 7.9$, the presence of paragonite prevents an accurate estimation of HI. R_2 (Figure 3b) clearly decreases with increasing pH_F , reflecting an increase of monoclinic character. The large standard deviation of the R_2 value

of the kaolinite synthesized at 240°C for $\text{pH}_F = 7.9$ is related to the presence of paragonite.

CS_{001} (Figure 4a) does not vary significantly to $\text{pH}_F = 5.5$ and seems to decrease slightly above this value. CS_{060} (Figure 4b) remains nearly constant to $\text{pH}_F = 6.5$. The apparent coherent scattering thickness estimated from samples synthesized at the most basic pH are less precise owing to less crystallization of the initial material into kaolinite.

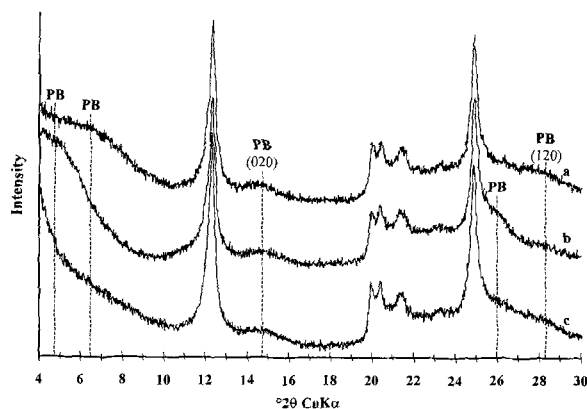


Figure 2. XRD patterns of the sample obtained at 220°C, for $\text{pH}_F = 8.4$: a) from an oriented preparation, placed overnight in an ethylene glycol-saturated atmosphere; b) from an oriented preparation without any treatment; and c) from an oriented preparation, heated at 120°C for 2 h. PB = Pseudo-boehmite.

DTA-TG

For each given pH_F , DTA curves of kaolinites synthesized at 200, 220, and 240°C are similar, therefore only DTA curves at 220°C are given in Figure 5. The low-temperature endothermic peak observed in the 50–100°C range for the starting material is related to dehydration of amorphous material. Kaolinite synthesized at $\text{pH}_F = 8.4$ also shows low-temperature (<100°C) endotherms. These endotherms are produced by sorbed H_2O on the residual product (at 50–60°C) and to dehydration of the (swelling) pseudo-boehmite described above (at 80°C). These endotherms suggest that the sample is poorly crystallized. This is confirmed by TG analysis which indicates that the product contained only 60–70% kaolinite.

The dehydroxylation endotherms (~500°C) are slightly asymmetric owing to populations of kaolinite

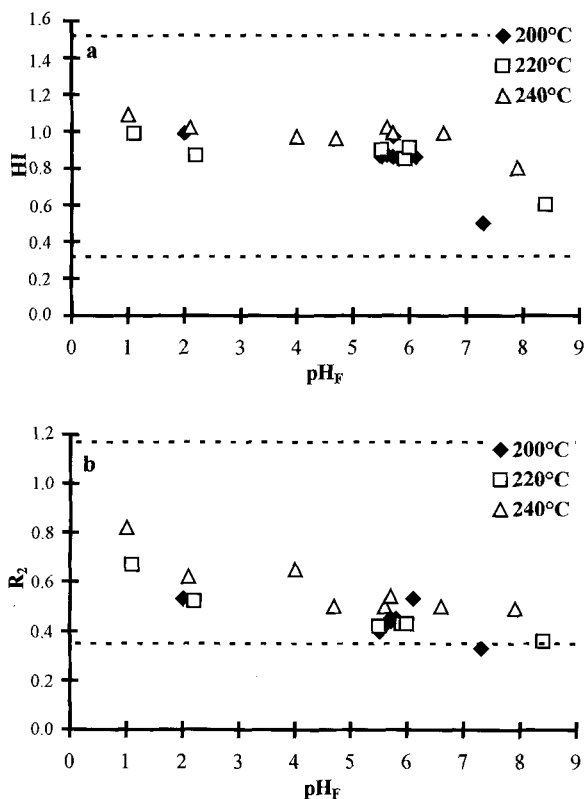


Figure 3. Variations of the "crystallinity" indexes of kaolinite based on the synthesis temperature and pH_F: a) HI and b) R₂. The error estimates are ≤ 0.1 pH units for syntheses with pH_F < 7 and ≤ 0.3 unit for syntheses with pH_F > 7. Dotted lines delineate the ranges of indexes of naturally occurring kaolinite according to Liétard (1977).

particles with different sizes (see TEM below) and defect densities. For pH_F = 1.1, the peak temperature of dehydroxylation (T_{\max}) of kaolinite is 516°C. T_{\max} progressively decreases with increasing pH_F, to 502°C for pH_F = 8.4. T_{\max} of the synthesized kaolinites is higher than that of the kaolinite contained in the starting material for all values of pH_F.

For the most acidic pH_F, the exothermic peak, corresponding to the spinel transition, is sharp and occurs at 996°C. For pH_F = 8.4, this peak is broad and occurs at 988°C. These temperatures are typical for synthetic kaolinites (e.g., Calvert, 1981; Petit *et al.*, 1995) and for low-defect natural kaolinites with low iron content (e.g., Calvert, 1981; Cases *et al.*, 1982).

TEM

Analysis of the synthesized products by TEM revealed substantial morphological differences of synthetic kaolinites as a function of pH_F. However, for each given pH_F, the morphology and particle size of the kaolinite synthesized at 200, 220, and 240°C are similar. Photographs of four samples, synthesized at

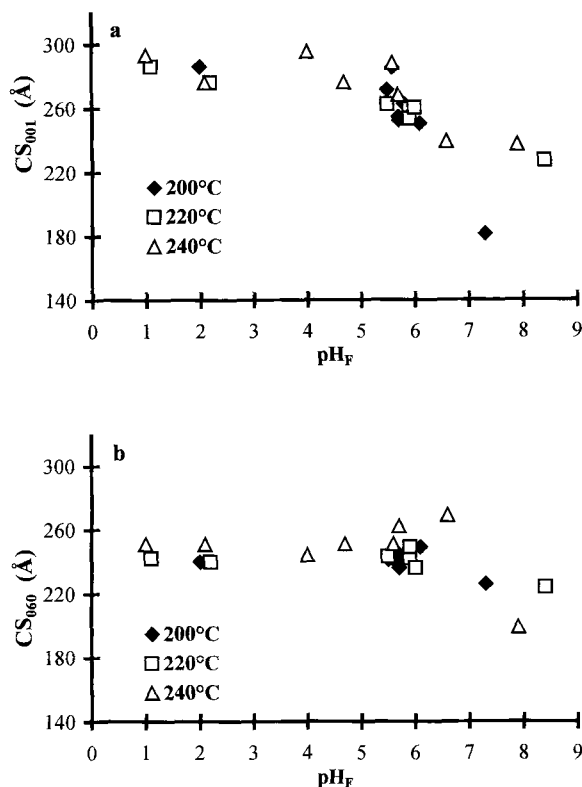


Figure 4. Variations of the apparent coherent scattering thickness of kaolinite based on the synthesis temperature and pH_F: a) along the c^* axis; and b) along the b axis using the (001) and (060) reflections. The error estimate is 20 Å for syntheses with pH_F < 7. For syntheses with pH_F > 7, error is not measurable accurately and is >20 Å. Error estimates for pH are ± 0.2 .

240°C for pH_F = 1.0, 4.7, 6.6, and 7.9 are shown in Figure 6.

A great number of large hexagonal plates is observed for the most acidic pH_F (Figure 6a). These plates appear to aggregate and remain nearly hexagonal, with diameters of 0.3–1.5 μm . For pH_F = 4.7 (Figure 6b), plates are often slightly elongated, with some lozengic or elongated pseudo-hexagonal shapes, and with a diameter from 0.2 to 0.7 μm . For pH_F = 6.6 (Figure 6c), plates are very elongated, and emanate from rose-shaped aggregates. These plates can reach $1.5 \times 0.15 \mu\text{m}$ in shape. For pH_F = 7.9 (Figure 6d), lath-shaped kaolinites appear as individual particles to $2.5 \times 0.25 \mu\text{m}$. At this pH_F, a residual gel is also observed.

AAS

Chemical analyses of the reaction products containing only kaolinite or traces of pseudoboehmite were performed by AAS. The number of Na atoms contained in several samples per two Si atoms is plotted in Figure 7 as a function of pH_F. The number of Na atoms significantly increases with pH_F.

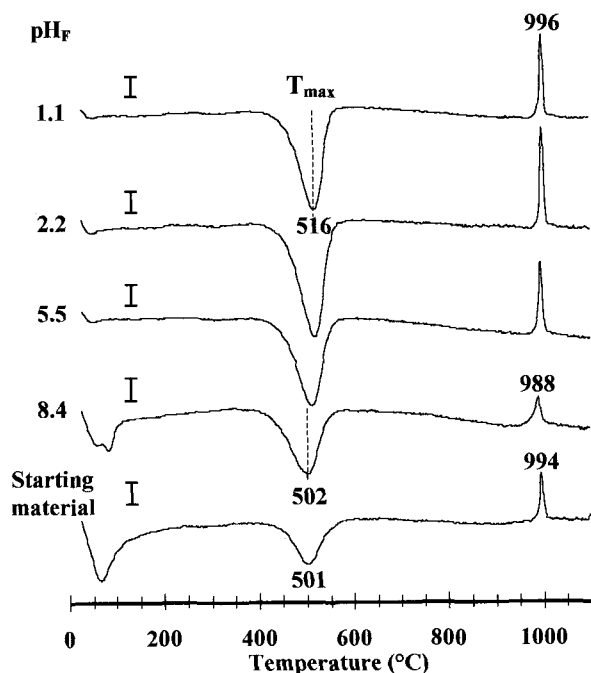


Figure 5. DTA curves of the starting material and of the kaolinites synthesized at 220°C according to pH_F . The vertical scale is 4 μV . Errors in temperature are $\pm 5^\circ\text{C}$.

FTIR

The FTIR spectra in the hydroxyl-stretching region for the kaolinite synthesized at 220°C are shown in Figure 8. The four characteristic hydroxyl bands of kaolinite are well resolved for $\text{pH}_F = 1.1$. The 3620- cm^{-1} band is caused by the inner-hydroxyl vibrations (e.g., Ledoux and White, 1964; Barrios *et al.*, 1977; Rouxhet *et al.*, 1977). The other bands, at 3693, 3668, and 3651 cm^{-1} , are related to the vibrations of the three inner-surface hydroxyls. The 3693 and 3668- cm^{-1} bands are attributed to coupled antisymmetric and symmetric vibrations (Farmer and Russell, 1964; Farmer, 1964, 1974). The attribution of the 3651- cm^{-1} band is still debated (Brindley *et al.*, 1986). However, according to data of Bish and Johnston (1993) it may be assigned to the combination of the OH_2 and OH_4 hydroxyl groups. These inner-surface hydroxyls have very similar environments and are believed to be nearly parallel to the c^* axis (Prost *et al.*, 1987; Johnston *et al.*, 1990). The 3651- cm^{-1} band is believed to correspond to the out-of-phase analogue of the in-phase vibration located at 3685 cm^{-1} , which is only active by Raman spectroscopy (Frost and Van Der Gaast, 1997).

As pH_F increases, the intensity of the 3668- cm^{-1} band decreases relative to the 3651- cm^{-1} band, reflecting an increase of monoclinic character of the kaolinite (Liétard, 1977; Brindley *et al.*, 1986). For $\text{pH}_F = 8.4$, defect density is sufficiently high that it is not possible

to distinguish between these bands. Moreover, for this sample, an infrared (IR) band is present as a shoulder near 3600 cm^{-1} . Since the starting material is iron free, this band cannot be attributed to AlFeOH vibrations, as attributed for natural and synthetic iron-substituted kaolinites (Petit and Decarreau, 1990; Delineau *et al.*, 1994). Furthermore, since the 3600- cm^{-1} band remains after heating at 120°C, this band is not related to swelling pseudoboehmite. Along with the OH bands, the shoulder disappears in samples heat treated above 400°C when heating KBr pellets progressively from 240 to 510°C, in increments of 30°C, for 2 h at each temperature. Thus, the 3600- cm^{-1} band cannot be explained by intercalated water (Kukovskii *et al.*, 1969).

For kaolinites synthesized at 220°C, the 3600- cm^{-1} shoulder is only visible for samples formed at $\text{pH}_F = 8.4$. The shoulder occurs also for the highest pH values for the experiments at 200 and 240°C ($\text{pH}_F = 7.3$ and 6.6, respectively). The shoulder may be present in the spectrum of the sample obtained for $\text{pH}_F = 7.9$ at 240°C, although paragonite may obscure this band. Furthermore, the intensity of the 3600- cm^{-1} shoulder is closely related to pH_F . For example, the intensity is higher at $\text{pH}_F = 8.4$ at 220°C than at $\text{pH}_F = 6.6$ at 240°C.

No difference is detected between FTIR spectra obtained from a given pH_F regardless of the temperature of synthesis. The spectra obtained for kaolinite synthesized at 200, 220, and 240°C with $\text{pH} = 5.5$ –5.7 are essentially identical. The OH configuration of the starting material formed at $\text{pH}_1 \sim 5$ and for the kaolinite synthesized at $\text{pH}_F = 5.5$ is similar (Figure 8).

The normalized FTIR spectra of ammonium-saturated samples are given in Figure 9 according to pH_F . The integrated intensity of the $\nu_4\text{NH}_4$ band located at 1400 cm^{-1} [$I(\nu_4\text{NH}_4)$] clearly increases according to pH_F (Figure 9). A perfect linear relationship is observed between $I(\nu_4\text{NH}_4)$ and the amount of sodium contained in the unsaturated samples, except for $\text{pH}_F = 8.4$ which is not sufficiently pure for comparison to the other samples (Figure 10). The shoulder described above at 3600 cm^{-1} is not affected by ammonium treatment.

DISCUSSION

Influence of pH on paragenesis

For $\text{pH}_F \sim 0.5$, the only product phase obtained was amorphous silica, according to the sequence: $\text{SiO}_2 \rightarrow \text{SiO}_2 + \text{Al}_2\text{Si}_2\text{O}_5(\text{OH})_4$, as described theoretically by Tsuzuki (1976) for K-rich feldspar alteration at 200°C and pH of 1.8. During dissolution of the starting material, the solution first reaches supersaturation of silica. At $\text{pH} \leq 1.8$, amorphous silica precipitates while aluminum, being highly soluble, may stay in solution. However, Satokawa *et al.* (1996) synthesized kaolinite at $\text{pH}_F = 0.4$ and 220°C after 10 d from silica gel and

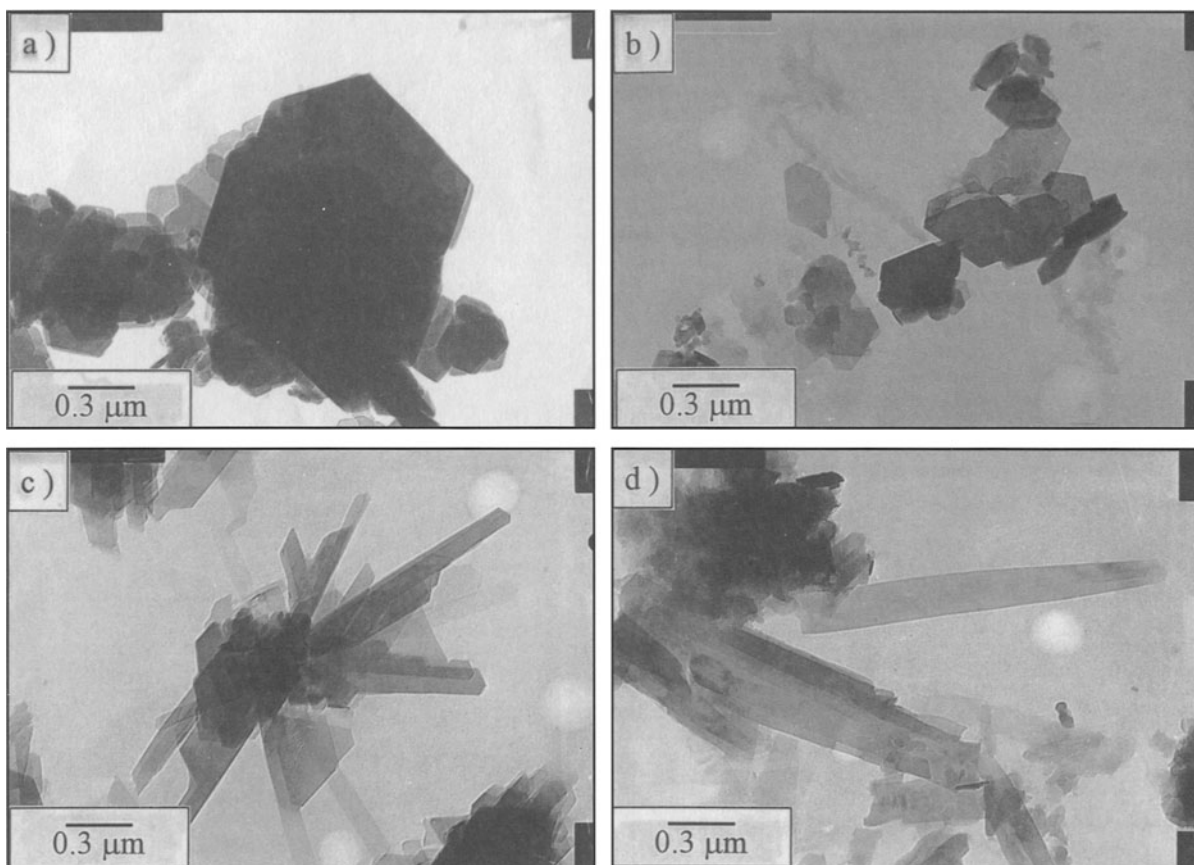


Figure 6. Transmission electron micrographs of kaolinites synthesized at 240°C for various pH_F values: a) $\text{pH}_F = 1.0$, b) $\text{pH}_F = 4.7$, c) $\text{pH}_F = 6.6$, and d) $\text{pH}_F = 7.9$.

gibbsite using a higher solid/solution ratio than those used for this study.

For pH_F in the range 1.0–6.1, kaolinite is the major phase present, often associated with pseudoboehmite. Using a thermodynamic approach, Tsuzuki (1976)

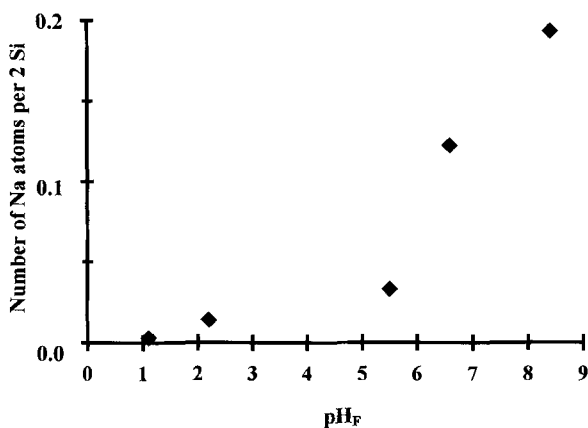


Figure 7. Number of sodium atoms contained in kaolinite sample (± 0.01) per two Si atoms according to pH_F . The error associated with pH_F is ± 0.2 .

showed that when K-rich feldspar is dissolved at 200°C and pH 4 in a closed system, the sequence of precipitation is: boehmite \rightarrow kaolinite \rightarrow amorphous silica + kaolinite. In this study, under similar temperature and pH conditions, boehmite occurred as a precursor to kaolinite. Boehmite will precipitate at an earlier stage of the synthesis and progressively “feed” kaolinite formation. Satokawa *et al.* (1994) obtained boehmite associated with platy kaolinite by hydrothermal synthesis from an amorphous gel. They proposed that platy-shape kaolinite will be “crystallized on the basis of the sheet structure of the boehmite”. The only kaolinite shapes observed in the present study were plates (more or less elongated) and the kaolinite was often associated with pseudoboehmite, providing additional evidence for the hypothesis of Satokawa *et al.* (1994).

Note that each synthesized kaolinite sample was obtained by complete transformation of the starting material. Despite the presence of $\sim 50\%$ of kaolinite of medium-defect density in the starting material, nearly 100% of kaolinite of low-defect density was obtained in 21 d for pH_F in the range 1.0–6.1, whereas $\sim 70\%$ of kaolinite of high-defect density was formed for pH_F

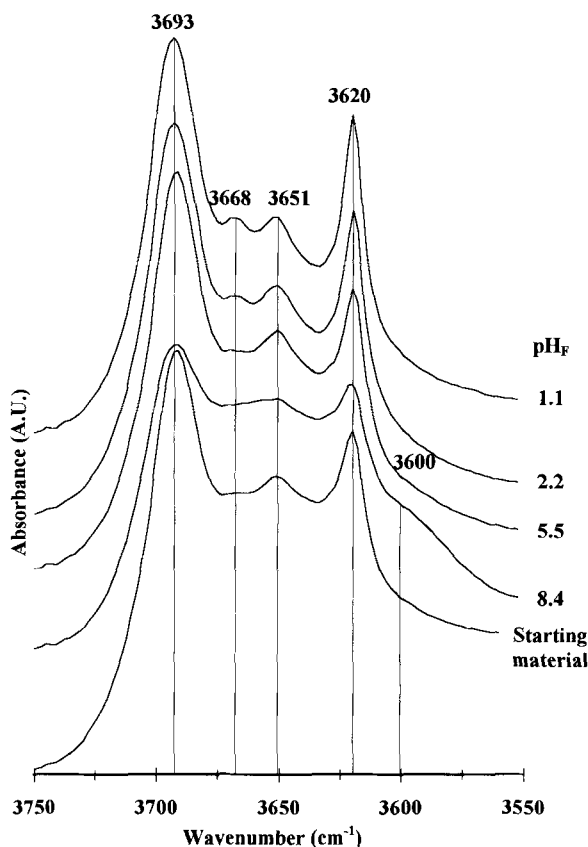


Figure 8. FTIR spectra in the OH-stretching region of the starting material and of the kaolinites synthesized at 220°C according to pH_F . A. U. = arbitrary unit.

in the range 6.6–8.4. Therefore, it is possible to form high-defect kaolinite from the dissolution of kaolinite with lower-defect density for experiments completed over relatively short durations.

Influence of pH_F on kaolinite “crystallinity”

The pH does not greatly affect the HI. However, although this index is sensitive to all crystalline defects of kaolinite, it is only a semi-quantitative determination. Indeed, the HI may be related to kaolinite grains with different numbers of defects in a sample rather than one defect density (Plançon *et al.*, 1988, 1989). The HI is similar for nearly all pH_F (nearly 1.0) and is slightly higher than the maximum obtained by Miyawaki *et al.* (1991) for kaolinite synthesized at 220°C for shorter synthesis times. These authors established a positive correlation between HI and kaolinite yield, and our results are identical. Satokawa *et al.* (1996) studied the effect of acidity on the hydrothermal formation of kaolinite from silica gel and gibbsite. These authors observed differences in the HI independently of pH_F . However, they used a shorter duration (10 d) and observed a decrease of the gibbsite dissolution rate as pH increases. No comparison can

be made with our study because of the differences of reactivity of starting materials and synthesis time.

The R_2 index is sensitive to all kaolinite defects except those of translation ($\pm b/3$) or rotation ($\pm 2\pi/3$) (Liétard, 1977; Cases *et al.*, 1982). R_2 decreases with the increase of pH_F and this denotes an increase in the number of C layers (*i.e.*, kaolinite layer with the vacancy located in the C octahedral site; see Bailey, 1980) among B-layer stacking (*i.e.*, kaolinite layer with the octahedral vacancy in the B site), and thus an increase of the monoclinic character of kaolinite. Furthermore, as previously established by Plançon *et al.* (1989) for natural kaolinites, the HI of the synthesized kaolinite is not related to monoclinic character, as the HI is constant whereas R_2 decreases.

Satokawa *et al.* (1996) obtained CS_{001} values >200 Å for $\text{pH}_F < 2$, and CS_{001} values <200 Å for higher pH. In the present study, CS_{001} is >200 Å for all pH_F (except for one sample). These differences are probably related to different synthesis conditions. The pH has only a weak or no effect on the kaolinite CS_{060} , as it is nearly constant for all pH_F .

The effect of pH on the hydroxyl configuration of synthesized kaolinites is very important. A continuous series is observed from a low-defect kaolinite for acidic pH_F to a kaolinite with a pronounced monoclinic character for the most basic pH_F . A similar series of IR spectra in the hydroxyl-stretching region was observed for Cu-substituted synthetic kaolinites (Petit *et al.*, 1995). By an IR study of natural kaolinite intercalated with hydrazine, Cruz-Cumplido *et al.* (1982) established that the disorder apparent in IR spectra is caused by the decrease of the angle between the OH groups and the c^* axis, which produces an increase in the interlamellar cohesion. Furthermore, they proposed that the OH orientation is a function of Al-vacancy distribution between adjacent sheets. In our case, variations in orientation of outer-hydroxyl groups are apparently related to the pH effect during kaolinite crystal growth and are correlated with R_2 as already observed for natural kaolinites by Liétard (1977). Therefore, increasing pH induces variations of the orientations of the outer-hydroxyl groups.

The high-defect density of natural kaolinites was commonly correlated to the amount of substituted iron; “crystallinity” and particle size of kaolinite samples decrease as the iron content increases (Mestdagh *et al.*, 1980, 1982; Cases *et al.*, 1982; Delineau *et al.*, 1994). In the present study, variations in the defect density and particle size of kaolinite are induced by pH. Thus, the high-defect density of natural kaolinites is not necessarily related to iron (or other cations) but, and probably essentially so, to the chemical aqueous conditions of kaolinite formation, with pH playing a major role.

The study of surface chemistry by FTIR

Devidal *et al.* (1992) and Xie and Walther (1992) studied the surface speciation of kaolinite at 25°C as a

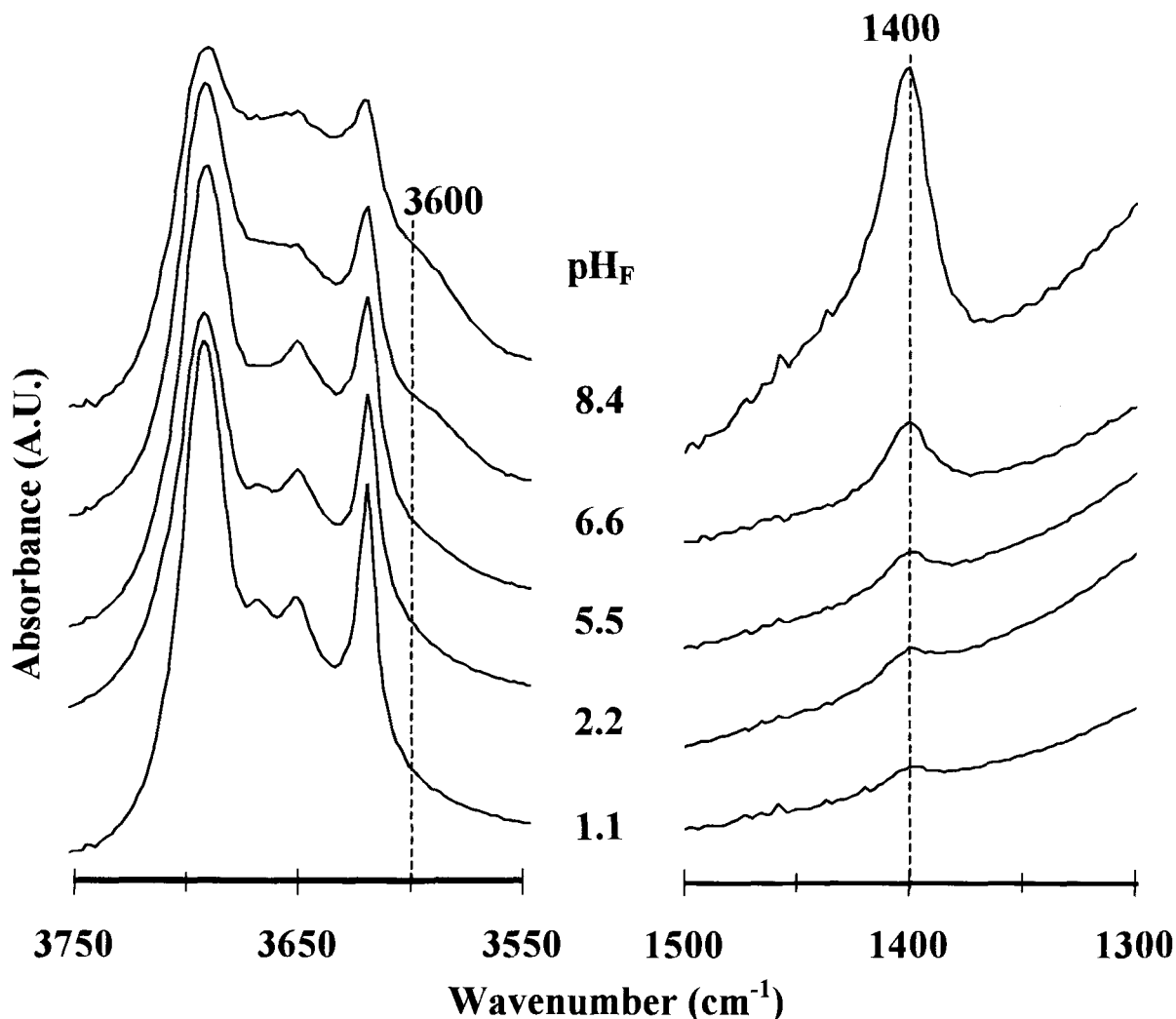


Figure 9. FTIR normalized spectra of ammonium-saturated samples according to pH_F .

function of pH. They established that in acidic solutions ($\text{pH} < 4$) the dominant surface species of kaolinite are Si-OH and Al(OH)_2^+ . As pH increases, the proportions of these species decrease whereas the proportions of the Si-O^- and Al-OH species increase. For increasing pH from 8 to 14, the proportion of the Al-OH surface species reaches a maximum and then decreases in favor of the Al-O^- species. Clearly, while kaolinites are in contact with salt solutions, increasing pH increased the amount of Na^+ adsorbed on the kaolinite lateral surfaces to form $\text{Si-O} \cdots \text{Na}$ linkages (Xie and Walther, 1992). Theoretically, $\text{Al-O} \cdots \text{Na}$ links may also form at basic pH ($\text{pH} > 10$ at 25°C ; Xie and Walther, 1992) but no kaolinite was obtained beyond $\text{pH}_F = 8.5$.

The intensity of the 3600-cm^{-1} shoulder increases with pH_F and decreases in intensity as hydroxyl groups are lost. Thus, the 3600-cm^{-1} shoulder may be generated by a perturbation of hydroxyl groups owing to

interactions with the cations adsorbed on the kaolinite surface. FTIR spectroscopy shows that the number of Na^+ cations associated with synthesized kaolinites is exchangeable by NH_4^+ . When NH_4^+ is linked to clay structures, the deformation band is located at 1440 cm^{-1} (Petit *et al.*, 1999). The band related to NH_4^+ observed in this study is located at 1400 cm^{-1} , indicating a total exchange of NH_4^+ ions from synthesized kaolinites with K^+ ions from KBr (Petit *et al.*, 1999). Pelletier *et al.* (1999) and Petit *et al.* (1999) showed that interlayer cations of smectites exchange also with K^+ from KBr pellets. Adsorbed cations on the external surfaces of synthetic kaolinites (NH_4^+ and also Na^+) are exchanged by K^+ in KBr pellets. The strong correlation between the intensities of the 1400 and 3600-cm^{-1} bands implies that adsorbed K^+ ions may be responsible for the 3600-cm^{-1} band observed for both unsaturated and NH_4 -saturated samples.

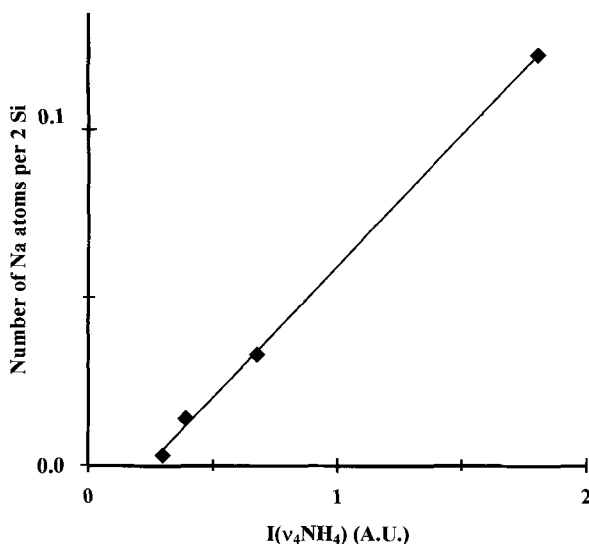


Figure 10. Number of sodium atoms per two Si atoms contained in the unsaturated samples according to the normalized integrated intensity of the NH_4^+ band of the ammonium-treated samples.

The increase with pH of cation adsorption on the kaolinite surface is closely linked to the increase of Si-O^- surface species, implying a positive correlation between the kaolinite surface charge and pH. Thus, it may be possible to estimate with good precision the cation-exchange capacity of any kaolinite by measuring $I(\nu_4\text{NH}_4)$ of the NH_4 -saturated samples, which is directly related to the amount of exchangeable cations (Petit *et al.*, 1999).

Influence of pH_F on the morphology of synthesized kaolinites

For $\text{pH}_F > 7$, kaolinite particles are in the shape of laths whereas for $\text{pH}_F \leq 6$, kaolinite particles show pseudohexagonal morphology. Some authors obtained lath particles of kaolinite but not as elongated as those of the present study (Petit and Decarreau, 1990; Fiore *et al.*, 1995). Much information on the kaolinite crystal-growth mechanisms may be obtained by a detailed study of kaolinite morphology. Fiore *et al.* (1995) established a scheme of formation of the different morphologies of kaolinite from silicoaluminous gels under hydrothermal conditions. They estimated that the lath morphology would be promoted by a higher supersaturation whereas the platy particles are favored by lower supersaturation. In the present study, although using the same solid/solution ratio, hexagonal particles are obtained for the most acidic pH and progressively, particles elongate with increasing pH_F value until becoming lath-like for the more basic pH_F . Such an evolution of morphology may be related to the conditions of solution saturation, which are pH dependent. However, owing to the increasing amount of sodium adsorbed

on the kaolinite surface according to pH_F , the progressive lengthening of hexagonal-like particles may be attributed to a poisoning of kaolinite crystal growth by sodium on several faces. Several authors (*e.g.*, Cases *et al.*, 1982) suggested that the decrease of kaolinite "crystallinity" and particle size with the increase of iron content observed for natural iron-substituted kaolinites may be related to poisoning of faces by impurities (*e.g.*, Fe, Li). This hypothesis seems to be confirmed by the present results as there is effectively a negative correlation between the defect density of the synthesized kaolinite and the increase in sodium adsorbed on the surface.

ACKNOWLEDGMENTS

The authors wish to thank M. Garais for performing the chemical analyses, the NH_4 -saturations, and the DTA-TG analyses of the samples. We also wish to thank the SIMIS Laboratory of Poitiers for permission to use the transmission electron microscope.

REFERENCES

- Bailey, S.W. (1980) Structure of layer silicates. In *Crystal Structures of Clay Minerals and Their X-ray Identification*, G.W. Brindley and G. Brown, eds., Mineralogical Society, London, 28–39.
- Barrer, R.M. and White, E.A.D. (1952) The hydrothermal chemistry of silicates. Part II. Synthetic crystalline sodium aluminosilicates. *Journal of the Chemical Society*, 1561–1571.
- Barrios, J., Plançon, A., Cruz, M.I., and Tchoubar, C. (1977) Qualitative and quantitative study of stacking faults in a hydrazine treated kaolinite—relationship with the infrared spectra. *Clays and Clay Minerals*, **25**, 422–429.
- Bish, D.L. and Johnston, C.T. (1993) Rietveld refinement and Fourier-transform infrared spectroscopic study of the dickite structure at low temperature. *Clays and Clay Minerals*, **41**, 297–304.
- Brindley, G.W. and Brown, G., eds. (1980) *Crystal Structures of Clay Minerals and Their X-ray Identification*. Mineralogical Society, London, 495 pp.
- Brindley, G.W. and Porter, A.R.D. (1978) Occurrence of dickite in Jamaica-ordered and disordered varieties. *American Mineralogist*, **63**, 554–562.
- Brindley, G.W., Kao, C.-C., Harrison, J.L., Lipsicas, M., and Raythatha, R. (1986) Relation between structural disorder and other characteristics of kaolinites and dickites. *Clays and Clay Minerals*, **34**, 239–249.
- Calvert, C.S. (1981) Chemistry and mineralogy of iron-substituted kaolinite in natural and synthetic systems. Ph.D. thesis, Texas A&M University, Texas, USA, 224 pp.
- Cases, J.M., Liétard, O., Yvon, J., and Delon, J.F. (1982) Etude des propriétés cristallographiques, morphologiques et superficielles de kaolinites désordonnées. *Bulletin de Minéralogie*, **105**, 439–457.
- Chatterjee, N.D. (1970) Synthesis and upper stability of paragonite. *Contributions to Mineralogy and Petrology*, **27**, 244–257.
- Cruz-Cumplido, M., Sow, C., and Fripiat, J.J. (1982) Spectre infrarouge des hydroxydes, cristallinité et énergie de cohésion des kaolins. *Bulletin de Minéralogie*, **105**, 493–498.
- De Kimpe, C., Gastuche, M.C., and Brindley, G.W. (1964) Low-temperatures syntheses of kaolin minerals. *American Mineralogist*, **49**, 1–16.
- Delineau, T., Allard, T., Muller, J.P., Barrès, O., Yvon, J., and Cases, J.M. (1994) FTIR reflectance vs. EPR studies of

- structural iron in kaolinites. *Clays and Clay Minerals*, **42**, 308–320.
- Devidal, J.L., Dandurand, J.L., and Schott, J. (1992) Dissolution and precipitation kinetics of kaolinite as a function of chemical affinity ($T = 150^{\circ}\text{C}$, $\text{pH} = 2$ and 7.8). In *Water-Rock Interaction*, Y.K. Kharaka and A.S. Maest, eds., Balkema, Rotterdam, 93–94.
- Eberl, D. and Hower, J. (1975) Kaolinite synthesis: The role of the Si/Al and (alkali)/(H^+) ratio in hydrothermal systems. *Clays and Clay Minerals*, **23**, 301–309.
- Espiau, P. and Pedro, G. (1984) Comportement des ions aluminiques et de la silice en solution: Étude de la formation de la kaolinite. *Clay Minerals*, **19**, 615–627.
- Farmer, V.C. (1964) Infrared absorption of hydroxyl groups in kaolinite. *Science*, **145**, 1189–1190.
- Farmer, V.C. (1974) The layer silicates. In *The Infrared Spectra of Minerals*, V.C. Farmer, ed., Mineralogical Society, London, 331–365.
- Farmer, V.C. and Russell, J.D. (1964) The infrared spectra of layer silicates. *Spectrochimica Acta*, **20**, 1149–1173.
- Fiore, S., Huertas, F.J., Huertas, F., and Linares, J. (1995) Morphology of kaolinite crystals synthesized under hydrothermal conditions. *Clays and Clay Minerals*, **43**, 353–360.
- Frost, R.L. and Van Der Gaast, S.J. (1997) Kaolinite hydroxyls—a Raman microscopy study. *Clay Minerals*, **32**, 471–484.
- Guinier, A. (1956) Diffraction par les cristaux de très petite taille. In *Théorie et Technique de la Radiocristallographie*, A. Guinier, ed., Dunod, Paris, 462–465.
- Hinckley, D.N. (1963) Variability in crystallinity values among the kaolin deposits of the coastal plain of Georgia and South Carolina. *Clays and Clay Minerals*, **11**, 229–235.
- Hlavay, J., Jonas, K., Elek, S., and Inczedy, J. (1977) Characterization of the particule size and the crystallinity of certain minerals by infrared spectrophotometry and other instrumental methods—I. Investigations on clay minerals. *Clays and Clay Minerals*, **25**, 451–456.
- Huertas, F.J., Huertas, F., and Linares, J. (1993) Hydrothermal synthesis of kaolinite: Method and characterization of synthetic materials. *Applied Clay Science*, **7**, 345–356.
- Jeanroy, E. (1974) Analyse totale par spectrométrie d'absorption atomique des roches, sols, minerais, ciments après fusion au métaborate de strontium. *Analysis*, **2**, 703–712.
- Johnston, C.T., Agnew, S.F., and Bish, D.L. (1990) Polarized single-crystal Fourier-transform infrared microscopy of Ouray dickite and Keokuk kaolinite. *Clays and Clay Minerals*, **38**, 573–583.
- Kukovskii, E.G., Plastinina, M.A., and Fedorenko, YU.G. (1969) Nature of water in layered silicates. II. Infrared spectroscopy of OH_n groups in 1:1 dioctahedral layers. *Konstituciã i Svoystva Mineraloy*, **3**, 17–25. (in Russian).
- La Iglesia Fernandez, A. and Martin Vivaldi, J.L. (1973) A contribution to the synthesis of kaolinite. In *Proceedings of the International Clay Conference, Madrid, 1972*, J.M. Serratos and A. Sánchez, eds., Division de Ciencias, Madrid, 173–184.
- Ledoux, R.L. and White, J.L. (1964) Infrared study of selective deuteration of kaolinite and halloysite at room temperature. *Science*, **145**, 47–49.
- Liétard, O. (1977) Contribution à l'étude des propriétés physicochimiques, cristallographiques et morphologiques des kaolins. Ph.D. thesis, University of Nancy, Nancy, France, 322 pp.
- Mestdagh, M.M., Vielvoye, L., and Herbillon, A.J. (1980) Iron in kaolinite: II. The relationship between kaolinite crystallinity and iron content. *Clay Minerals*, **15**, 1–13.
- Mestdagh, M.M., Herbillon, A.J., Rodrigue, L., and Rouxhet, P.G. (1982) Evaluation du rôle du fer structural sur la cristallinité des kaolinites. *Bulletin de Minéralogie*, **105**, 457–466.
- Miyawaki, R., Tomura, S., Samejima, S., Okazaki, M., Mizuta, H., Muruyama, S.I., and Shibasaki, Y. (1991) Effects of solution chemistry on the hydrothermal synthesis of kaolinite. *Clays and Clay Minerals*, **39**, 498–508.
- Nakamoto, K. (1963) Tetrahedral and square-planar five-atom molecules. In *Infrared Spectra of Inorganic and Coordination Compounds*, K. Nakamoto, ed., John Wiley and Sons, New York, 103–114.
- Pampuch, R. (1966) Infrared study of thermal transformations of kaolinite and the structure of metakaolin. *Prace Mineralogiczne*, **6**, 53–70.
- Pelletier, M., Michot, L.J., Barrès, O., Humbert, B., Petit, S., and Robert, J.L. (1999) Influence of KBr conditioning on the IR hydroxyl stretching region of saponites. *Clay Minerals*, **34**, 439–445.
- Petit, S. and Decarreau, A. (1990) Hydrothermal (200°C) synthesis and crystal chemistry of iron-rich kaolinites. *Clay Minerals*, **25**, 181–196.
- Petit, S., Decarreau, A., Mosser, C., Ehret, G., and Grauby, O. (1995) Hydrothermal synthesis (250°C) of copper-substituted kaolinites. *Clays and Clay Minerals*, **43**, 482–494.
- Petit, S., Righi, D., Madejová, J., and Decarreau, A. (1999) Interpretation of the infrared NH_4^+ spectrum of the NH_4^+ -clays: Application to the evaluation of the layer-charge. *Clay Minerals*, **34**, 543–549.
- Plançon, A. and Tchoubar, C. (1977) Determination of structural defects in phyllosilicates by X-ray powder diffraction—II. Nature and proportion of defects in natural kaolinites. *Clays and Clay Minerals*, **25**, 436–450.
- Plançon, A., Giese, R.F., and Snyder, R. (1988) The Hinckley index for kaolinites. *Clay Minerals*, **23**, 249–260.
- Plançon, A., Giese, R.F., Jr., Snyder, R., Drits, V.A., and Bookin, A.S. (1989) Stacking faults in the kaolin-group minerals: Defect structures of kaolinite. *Clays and Clay Minerals*, **37**, 203–210.
- Prost, R., Damême, A., Huard, E., and Driard, J. (1987) Infrared study of structural OH in kaolinite, dickite and nacrite at 300 to 5K. In *Proceedings of the International Clay Conference, Denver, 1985*, L.G. Schultz, H. van Olphen, and F.A. Mumpton, eds., The Clay Minerals Society, Bloomington, Indiana, 17–23.
- Rayner, J.H. (1962) An examination of the rate of formation of kaolinite from co-precipitated silica gel. In *Genèse et Synthèse des Argiles*, Centre National de la Recherche Scientifique, ed., Colloques Internationaux du Centre National de la Recherche Scientifique, Paris, **105**, 123–127.
- Rouxhet, P.G., Samudacheata, N., Jacogs, H., and Anton, O. (1977) Attribution of the OH stretching bands of kaolinite. *Clay Minerals*, **12**, 171–179.
- Satokawa, S., Osaki, Y., Samejima, S., Miyawaki, R., Tomura, S., Shibasaki, Y., and Sugahara, Y. (1994) Effects of the structure of silica-alumina gel on the hydrothermal synthesis of kaolinite. *Clays and Clay Minerals*, **42**, 288–297.
- Satokawa, S., Miyawaki, R., Osaki, Y., Tomura, S., and Shibasaki, Y. (1996) Effects of acidity on the hydrothermal synthesis of kaolinite from silica-gel and gibbsite. *Clays and Clay Minerals*, **44**, 417–423.
- Stubican, V. and Roy, E. (1961) Isomorphous substitution and infrared spectra of the layer lattice silicates. *American Mineralogist*, **46**, 32–51.
- Tettenhorst, R. and Hofmann, D.A. (1980) Crystal chemistry of boehmite. *Clays and Clay Minerals*, **28**, 373–380.
- Tomura, S., Shibasaki, Y., Mizuta, H., and Kitamura, M. (1985) Growth conditions and genesis of spherical and platy kaolinite. *Clays and Clay Minerals*, **33**, 200–206.

- Tsuzuki, Y. (1976) Solubility diagrams for explaining zone sequences in bauxite, kaolin and pyrophyllite-diaspore deposits. *Clays and Clay Minerals*, **24**, 297–302.
- Van Oosterwyck-Gastuche, M.C. and La Iglesia, A. (1978) Kaolinite synthesis. II. A review and discussion of the factors influencing the rate process. *Clays and Clay Minerals*, **26**, 409–417.
- Vedder, W. (1965) Ammonium in muscovite. *Geochimica et Cosmochimica Acta*, **29**, 221–228.
- Xie, Z. and Walther, J.V. (1992) Incongruent dissolution and surface area of kaolinite. *Geochimica et Cosmochimica Acta*, **56**, 3357–3363.

E-mail of corresponding author: sabine.petit@hydrasa.univ-poitiers.fr

(Received 5 October 1998; accepted 21 September 1999; Ms. 98-122)